Publ. Astron. Soc. Japan (2021) 73 (5), 1280–1288
https://doi.org/10.1093/pasj/psab074
Advance Access Publication Date: 2021 July 24

BO Ceti: Dwarf nova showing both IW And-type and SU UMa-Type features

Taichi Kato,[1,*] Yusuke Tampo,[1] Naoto Kojiguchi,[1] Masaaki Shibata,[1] Junpei Ito,[1] Keisuke Isogai,[2,3] Hiroshi Itoh,[4] Franz-Josef Hambsch,[5,6,7] Berto Monard,[8,9] Seiichiro Kiyota,[10] Tonny Vanmunster,[11,12] Aleksei A. Sosnovskij,[13] Elena P. Pavlenko,[13] Pavol A. Dubovsky,[14] Igor Kudzej,[14] and Tomas Medulka[14]

[1]Department of Astronomy, Kyoto University, Kitashirakawa-Oiwake-cho, Sakyo-ku, Kyoto, Kyoto 606-8502, Japan
[2]Okayama Observatory, Kyoto University, 3037-5 Honjo, Kamogatacho, Asakuchi, Okayama 719-0232, Japan
[3]Department of Multi-Disciplinary Sciences, Graduate School of Arts and Sciences, The University of Tokyo, 3-8-1 Komaba, Meguro, Tokyo 153-8902, Japan
[4]Variable Star Observers League in Japan (VSOLJ), 1001-105 Nishiterakata, Hachioji, Tokyo 192-0153, Japan
[5]Groupe Européen d'Observations Stellaires (GEOS), 23 Parc de Levesville, 28300 Bailleau l'Evêque, France
[6]Bundesdeutsche Arbeitsgemeinschaft für Veränderliche Sterne (BAV), Munsterdamm 90, 12169 Berlin, Germany
[7]Vereniging Voor Sterrenkunde (VVS), Oostmeers 122 C, 8000 Brugge, Belgium
[8]Bronberg Observatory, Center for Backyard Astrophysics Pretoria, PO Box 11426, Tiegerpoort 0056, South Africa
[9]Kleinkaroo Observatory, Center for Backyard Astrophysics Kleinkaroo, Sint Helena 1B, PO Box 281, Calitzdorp 6660, South Africa
[10]VSOLJ, 7-1 Kitahatsutomi, Kamagaya, Chiba 273-0126, Japan
[11]Center for Backyard Astrophysics Belgium, Walhostraat 1A, B-3401 Landen, Belgium
[12]Center for Backyard Astrophysics Extremadura, e-EyE Astronomical Complex, 06340 Fregenal de la Sierra, Badajoz, Spain
[13]Federal State Budget Scientific Institution "Crimean Astrophysical Observatory of RAS", Nauchny, 298409, Republic of Crimea
[14]Vihorlat Observatory, Mierova 4, 06601 Humenne, Slovakia

*E-mail: tkato@kusastro.kyoto-u.ac.jp

Received 2021 April 2; Accepted 2021 June 28

Abstract

IW And stars are a recently recognized subgroup of dwarf novae which are characterized by (often repetitive) slowly rising standstills terminated by brightening, but the exact mechanism for this variation is not yet identified. We have identified BO Cet, which had been considered as a novalike cataclysmic variable, as a new member of IW And stars based on its behavior in 2019–2020. In addition to this, the object showed dwarf nova-type outbursts in 2020–2021, and superhumps that had periods 7.8% longer than the orbital one developed during at least one long outburst. This object has been confirmed as an

SU UMa-type dwarf nova with an exceptionally long orbital period (0.1398 d). BO Cet is thus the first cataclysmic variable showing both SU UMa-type and IW And-type features. We obtained a mass ratio (q) of 0.31–0.34 from the superhumps in the growing phase (stage A superhumps). At this q, the radius of the 3 : 1 resonance, responsible for tidal instability and superhumps, and the tidal truncation radius are very similar. We interpret that in some occasions this object showed IW And-type variation when the disk size was not large enough, but that the radius of the 3 : 1 resonance could be reached as a result of thermal instability. We also discuss that there are SU UMa-type dwarf novae above $q = 0.30$, which is above the previously considered limit ($\sim$0.25) derived from numerical simulations and that this is possible since the radius of the 3 : 1 resonance is inside the tidal truncation radius. We constrained the mass of the white dwarf larger than 1.0 $M_{\odot}$, which may be responsible for the IW And-type behavior and the observed strength of the He II emission. The exact reason, however, why this object is unique in that it shows both SU UMa-type and IW And-type features is still unsolved.

Key words: accretion, accretion disks — novae, cataclysmic variables — stars: dwarf novae — stars: individual (BO Ceti)

1 Introduction

Cataclysmic variables (CVs) are close binaries consisting of a white dwarf (primary) and a mass-transferring red or brown dwarf forming an accretion disk. In some CVs, thermal instability in the accretion disk causes outbursts, and these CVs are called dwarf novae (DNe) [see, e.g., Osaki (1996); for general information of cataclysmic variables and dwarf novae, see, e.g., Warner (1995)]. There are three classical subclasses of DNe: SS Cyg stars with only normal outbursts, Z Cam stars showing both normal outbursts and standstills, and SU UMa stars showing normal outbursts and superoutbursts, during which superhumps with periods a few percent longer than the orbital period ($P_{\rm orb}$) are present.

Standstills in Z Cam stars are considered to be equivalent to novalike (NL) stars, in which the disks are thermally stable. It is widely believed that Z Cam stars have relatively high mass-transfer rates and that the accretion disk is considered to be close to the thermal stability. It is thought that a subtle variation in the mass-transfer rate from the secondary causes transitions between outbursting state and standstills (Meyer & Meyer-Hofmeister 1983). The exact mechanism, however, of the production of standstills is still not understood.

In recent years, a group of Z Cam stars which show unusual features has been identified (Simonsen 2011). This group is currently called IW And stars (Kato 2019).[1] The features special to IW And stars are (1) (quasi-)standstills terminated by brightening, not by fading as in "textbook" Z Cam stars, (2) sequences that are often very regular with almost a constant recurrence time (typically $\sim$30–100 d) and (3) deep dips which are sometimes seen following brightening. Two numerical models have been proposed to explain the IW And-type phenomenon: cyclic enhancement of mass-transfer rates from the secondary (Hameury & Lasota 2014), and a modification of the standard thermal instability model by considering the mass supply to the inner region of the disk (Kimura et al. 2020b). Although both models partially reproduced the IW And-type light curves, they could not explain the radius increase during (quasi-) standstills which are required by observation (Kimura et al. 2020a; M. Shibata et al. in preparation).

On the other hand, there is a rare DN, NY Ser, which is at the same time an SU UMa star and a Z Cam star (Kato et al. 2019). Two standstills in NY Ser were terminated by superoutbursts, which indicates that the disk radius can increase during standstills and eventually reach the 3 : 1 resonance. This object provides the clearest evidence that the disk radius can grow during standstills, which has not yet been realized in numerical simulations.

Here we report observations of BO Cet, which has shown distinct states: a long-lasting NL state, an IW And-type dwarf nova state, and SU UMa-type superoutbursts. There has been no other known object that shows both IW And and SU UMa states.

2 BO Cet

According to the General Catalog of Variable Stars (Samus et al. 2011), BO Cet was recognized as an NL star by R. Remillard in 1992, but without a solid reference. Zwitter and Munari (1995) obtained a spectrum and confirmed the NL nature. Rodríguez-Gil, Schmidtobreick, and Gänsicke (2007b) performed a more detailed spectroscopic study

[1] They are also called "anomalous Z Cam stars" (cf. Hameury & Lasota 2014).

and classified it as a non-eclipsing SW Sex star [see, e.g., Thorstensen et al. (1991) and Rodríguez-Gil et al. (2007a) for the description of SW Sex stars]. An orbital period of 0.13980 d was obtained by photometry by the members of the Center for Backyard Astrophysics and was refined to be 0.13983 d by Bruch (2017).[2] Lima et al. (2021) obtained time-resolved photometry and polarimetry, yielding a possible spin period of 11.1 min by variation of the circular polarization. Lima et al. (2021) detected a photometric period of 19.7 min. Nearly the same period was also detected by radial velocities of the Hα line wings (Rodríguez-Gil et al. 2007b).

During the early history of the research of BO Cet, this object was considered as an NL star. Indeed, ASAS-3 (Pojmański 2002) and available AAVSO observations did not show large variations in between 2001 and 2010.[3] During the course of a systematic study of CVs using Gaia DR2 (Gaia Collaboration 2018) and the All-Sky Automated Survey for Supernovae (ASAS-SN) Sky Patrol (Shappee et al. 2014; Kochanek et al. 2017), one of the authors (T.K.) noticed that this object showed dwarf nova states in late 2013 and 2017 November to December (vsnet-chat 8150,[4] E-figure 1).[5] In 2020 June, the object was found to be in IW And state since 2019 July (see subsection 4.1) using the ASAS-SN data (vsnet-alert 24387),[6] and a campaign was launched.

3 Observations and analysis

The CCD time-series observations were obtained in eight locations between 2020 June and 2021 March under a campaign led by the VSNET Collaboration (Kato et al. 2004) which comprised 30-cm class telescopes. The data analysis was performed in the same way as described in Kato et al. (2009) and Kato et al. (2014) and we mainly used R software for data analysis.[7] In period analysis, we de-trend the data by using both linear fitting and locally weighted polynomial regression (LOWESS: Cleveland 1979) on 2–38 d segments to remove outburst trends depending on the complexity of the light curve. The times of superhump maxima were determined by the template fitting method as described in Kato et al. (2009). The times of all observations are expressed in barycentric Julian days (BJD).

[2] J. Patterson in 2002 ⟨https://cbastro.org/pipermail/cba-public/2002-October/000300.html⟩.

[3] ⟨http://www.aavso.org/data-download⟩.

[4] ⟨http://ooruri.kusastro.kyoto-u.ac.jp/mailarchive/vsnet-chat/8150⟩.

[5] E-figures 1–2 and e-table 1 are available in the supplementary data section of the online edition of this article.

[6] ⟨http://ooruri.kusastro.kyoto-u.ac.jp/mailarchive/vsnet-alert/24387⟩.

[7] The R Foundation for Statistical Computing ⟨http://cran.r-project.org/⟩.

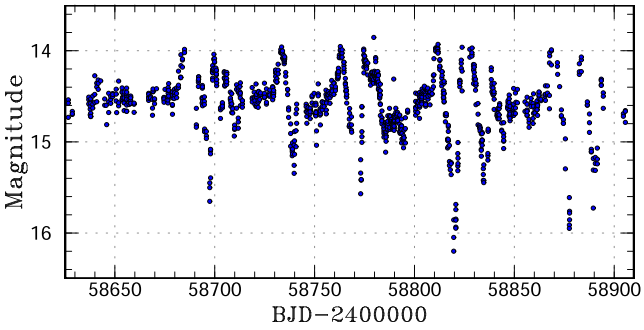

Fig. 1. *g*-band light curve of BO Cet during the 2019–2020 season from the ASAS-SN archive. This season started with a standstill or NL state which likely persisted since 2016 December (observations were interrupted by solar conjunctions) until BJD 2458680. This standstill or NL state was terminated by brightening in BJD 2458680–2458685. Two well-defined IW And-type cycles are seen between BJD 2458710 and 2458770: slowly rising standstills terminated by brightening followed by deep dips. Other instances of termination of standstill by brightening are seen around BJD 2458810 and 2458868. (Color online)

We used phase dispersion minimization (PDM; Stellingwerf 1978) for period analysis, and 1σ errors for the PDM analysis were estimated using the methods of Fernie (1989) and Kato et al. (2010).

We also obtained a snapshot spectrum between BJD 2459157.9699 and 2459157.9856 using the Kyoto Okayama Optical Low-dispersion Spectrograph with an Integral Field Unit (KOOLS-IFU; Matsubayashi et al. 2019) mounted on the 3.8-m telescope Seimei at Okayama Observatory, Kyoto University (Kurita et al. 2020). The wavelength coverage of VPH-Blue of KOOLS-IFU is 4200–8000 Å, and its wavelength resolution is $R = \lambda/\Delta\lambda = 400$–600. The data reduction was performed using IRAF in the standard manner (bias subtraction, flat fielding, aperture determination, scattered light subtraction, spectral extraction, wavelength calibration with arc lamps, and normalization by the continuum).

4 Results

4.1 2019–2020 season: IW And phase

The ASAS-SN light curve of the 2019–2020 season (2019 May to 2020 February) is shown in figure 1. This season started with a standstill or an NL state which likely persisted since 2016 December (observations were interrupted by solar conjunctions) until BJD 2458680. This standstill or NL state was terminated by brightening in BJD 2458680–2458685. Two well-defined IW And-type cycles are seen between BJD 2458710 and 2458770: slowly rising standstills terminated by brightening followed by deep dips. Other instances of termination of standstill by brightening

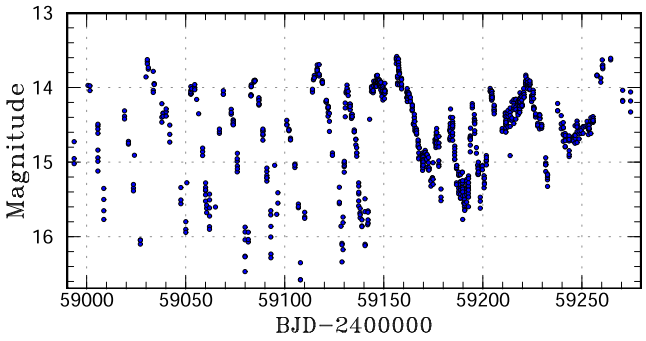

Fig. 2. *g*-band light curve of BO Cet during the 2020–2021 season from the ASAS-SN archive. The object showed dwarf nova-type outbursts until BJD 2459140 and no IW And-type feature was present. (Color online)

are seen around BJD 2458810 and 2458868. All these features support the classification of BO Cet as an IW And star (Kato 2019).

4.2 2020–2021 season: SU UMa/IW And phase

The ASAS-SN light curve of the 2020–2021 season (2020 May to 2021 February) is shown in figure 2. The object showed dwarf nova-type outbursts until BJD 2459140 and no IW And-type feature was present. Starting from BJD 2459144, the object reached a plateau, which was much brighter than standstills in the 2019–2020 season. Time-resolved photometry recorded growing superhumps during this plateau (subsection 4.4). After then, the object further brightened. After reaching the peak at $g = 13.6$, the object started fading slowly. As shown later, this part was identified as a superoutburst. Superhumps disappeared after this superoutburst and four small outbursts occurred (BJD 2459176–2459205), followed by a slowly rising standstill (BJD 2459209–2459222). Although less marked than in the 2019–2020 season, this standstill was terminated by weak brightening. The object again entered a slowly rising standstill (BJD 2459243–2459256) terminated by brightening (BJD 2459257–). Although the data were limited, this brightening was probably accompanied by superhumps and was likely a superoutburst.

In conclusion, the 2020–2021 season was a combination of SU UMa and IW And states. Such behavior was the first recorded among all known CVs.

4.3 Orbital signal

Using all the data from the VSNET Collaboration, we obtained a photometric orbital period of 0.139835 d, which is in very good agreement with Bruch (2017). The phase-averaged light curve clearly indicates that the object is eclipsing (depth 0.09 mag) accompanied by a prominent

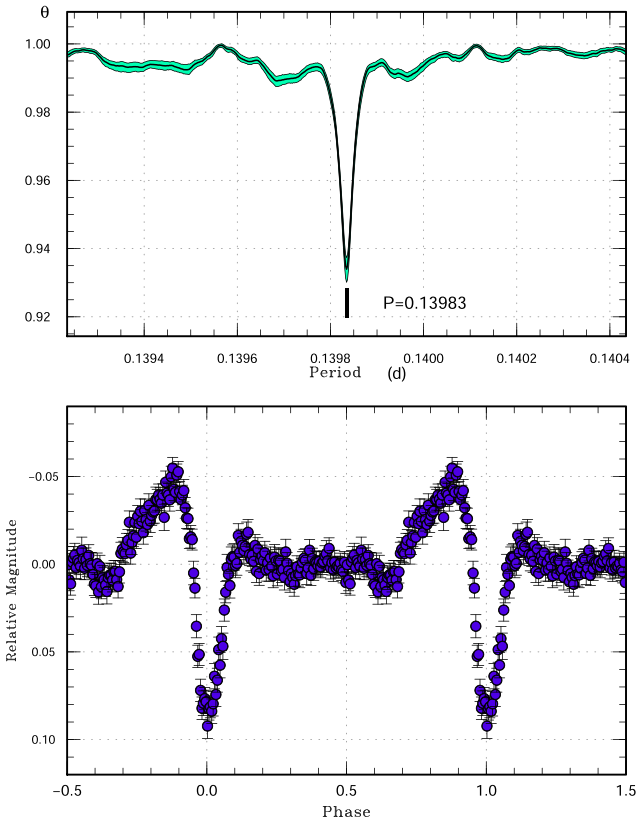

Fig. 3. Orbital signal of BO Cet. Upper: PDM analysis. We analyzed 100 samples which randomly contain 50% of observations, and performed the PDM analysis for these samples. The bootstrap result is shown as a form of 90% confidence intervals in the resultant PDM θ statistics. Lower: Phase-averaged profile. A shallow eclipse and an orbital hump are clearly seen. 1σ error bars are shown. (Color online)

orbital hump (figure 3). We have combined these data with ASAS-SN observations during the NL (or long standstill) phase in 2014–2019 and improved the period by Markov Chain Monte Carlo (MCMC) modeling of eclipses described in Kato et al. (2013). The eclipse ephemeris is

$$\mathrm{Min(BJD)} = 2459104.97794(9) + 0.13983546(3)E. \quad (1)$$

The presence of a prominent orbital hump appears to be inconsistent with the SW Sex-type classification (Rodríguez-Gil et al. 2007b), since prominent orbital humps are not usually seen in SW Sex stars (Thorstensen et al. 1991).

We could not detect any coherent signals around 11.1 min or 19.7 min claimed by Lima et al. (2021). If one of these periods reflects the spin period of the magnetized white dwarf (intermediate polar, IP), such a period should have been easily detected as a coherent signal in our observational condition with dense and long-term coverage [see, e.g., Kato et al. (2015) for an example of detection of an IP signal during a superoutburst under the similar observational set-up]. We consider that the periods detected

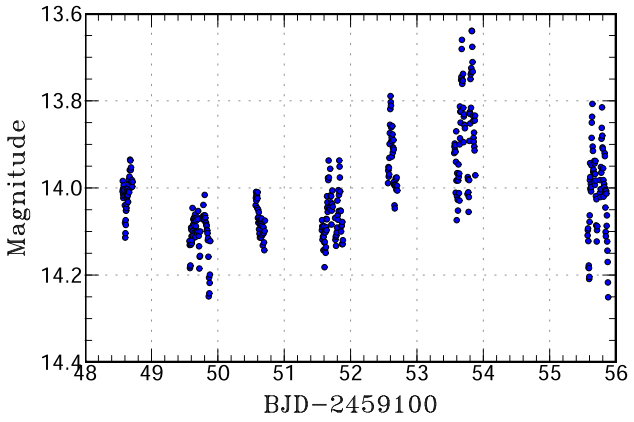

Fig. 4. Growing superhumps in BO Cet. The data were binned to 0.003 d. (Color online)

by Lima et al. (2021) were more likely quasi-periodic oscillations.

4.4 Superhumps and mass ratio

Superhumps appeared somewhere between BJD 2459144 and 2459151, and became prominent around BJD 2459154 (figure 4). The times of superhump maxima are listed in E-table 1. Since the superhump period is long, it was rather difficult to cover the sufficient phases of superhumps. Although variations were apparent to the eyes, some superhump maxima, particularly during the growing phase, were not determined. The $O-C$ curve and amplitudes of the initial part, however, are sufficient to show the growing phase (stage A, Kato et al. 2009) of superhumps (figure 5).

A two-dimensional PDM analysis is shown in figure 6. This figure corresponds to the two-dimensional discrete Fourier transform or least absolute shrinkage and selection operator (Lasso) analysis employed in Osaki and Kato (2013). In the case of BO Cet, PDM analysis gave a better result due to the non-sinusoidal nature of superhumps and nightly observational gaps. The resolution of PDM analysis is intermediate between Fourier transform and Lasso analysis, and this result can be treated as a slightly degraded version of Lasso analysis presented in Osaki and Kato (2013). The orbital signal was present most of the time. The frequency around 6.7 cycle d^{-1} (c/d) around BJD 2459160 represents superhumps. The signal with rapidly increasing frequencies prior to this corresponds to stage A superhumps. No signal of negative superhumps was present.

A PDM analysis of the interval BJD 2459151–2459166 yielded a mean superhump period of 0.15069(3) d, 7.8% longer than the orbital one.

We measured the period of superhumps during stage A by using two different segments: 0.1529(3) d for BJD

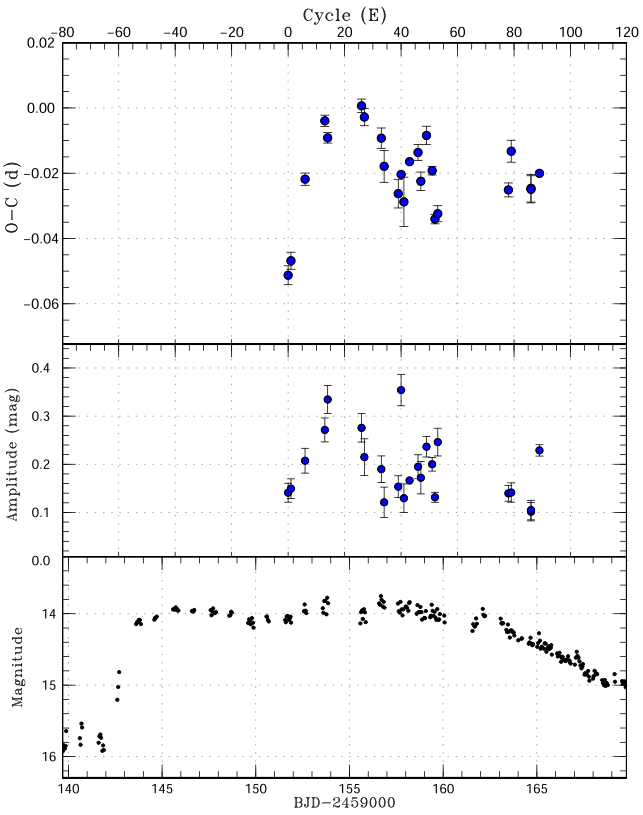

Fig. 5. $O-C$ diagram of superhumps in BO Cet. Upper: $O-C$ diagram. We used a period of 0.1507 d for calculating the $O-C$ residuals. Middle: Amplitudes of superhumps. Lower: Light curve. The data were binned to 0.05 d. During the segment $0 \leq E \leq 14$, the period was long and the amplitudes were rapidly growing. This segment corresponds to stage A. (Color online)

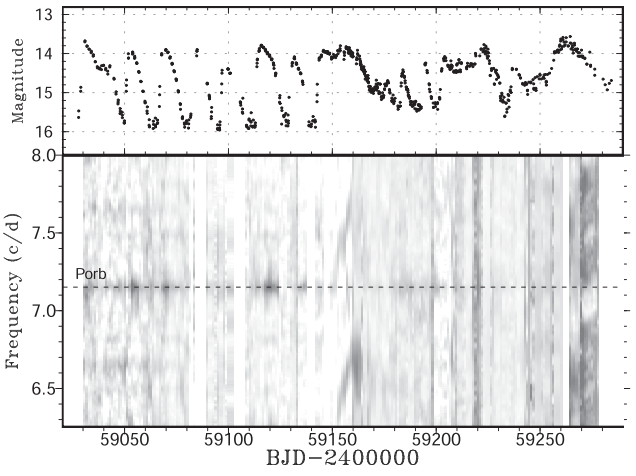

Fig. 6. Two-dimensional PDM analysis. Top panel: Light curve; the data were binned to 0.1 d, Bottom panel: Two-dimensional PDM analysis. 4-d segments shifted by 1 d were analyzed. Dark colors represent signals (lower θ in the PDM statistics). The orbital signal was present most of the time. The frequency around 6.7 c d^{-1} around BJD 2459160 represents superhumps. The signal with rapidly increasing frequencies prior to this corresponds to stage A superhumps. The weak signal around 7.5–7.7 c d^{-1} in BJD 2459150–2459160 is a one-day alias of the true frequency.

Table 1. Orbital inclination determined by eclipse modeling.

		Mass ratio q	
		0.31	0.34
Disk radius	0.30A	73°	72°
	0.46A	72°	71°

2459152–2459154 and 0.1541(2) d for BJD 2459150–2459154 with the PDM method. These values correspond to $\epsilon^* \equiv 1 - P_{\rm orb}/P_{\rm SH} = 0.085(2)$ and 0.092(1), where $P_{\rm SH}$ denotes the superhump period. According to Kato and Osaki (2013), the precession rate ϵ^* during stage A can be directly translated into q since the pressure effect is considered to be neglected. The above values correspond to $q = 0.31(1)$ and 0.0335(4), respectively. Considering the uncertainty in observationally determining when superhumps started to grow, we adopted $q = 0.31$–0.34 from this superhump analysis.

4.5 Mass of the white dwarf

We also modeled the eclipse profile assuming a standard disk with a surface brightness proportional to $r^{-0.75}$. The disk radius was assumed to be between an extreme values 0.30A, where A is the binary separation, and the tidal truncation radius. The real disk should be somewhere between them. For $q = 0.31$–0.34, we obtained an inclination of $i = 71°$–$73°$ (table 1). This value is not very dependent on the assumed power index and we adopted a value of $i = 72(1)°$. This value is significantly higher than $i = 35°$–$52°$ given in Rodríguez-Gil et al. (2007b).

The mass function is defined as

$$\frac{(M_1 \sin i)^3}{(M_1 + M_2)^2} = \frac{P_{\rm orb} K_2^3}{2\pi G}, \tag{2}$$

where K_2 is the semi-amplitude of the radial-velocity variations of the secondary component. In BO Cet, Rodríguez-Gil et al. (2007b) did not detect absorption lines of the secondary and used an emission-line component corresponding to the motion of the secondary in the Doppler tomogram. This observed semi-amplitude of the radial-velocity variations ($K_{\rm irr} = 262\,{\rm km\,s^{-1}}$) does not represent the motion of the mass center of the secondary, but that of the light center of the irradiated region in the secondary's surface. Thus $K_{\rm irr}$ is always smaller than K_2.

There is a relation

$$K_2 = \frac{K_{\rm irr}}{1 - f(1+q)}, \tag{3}$$

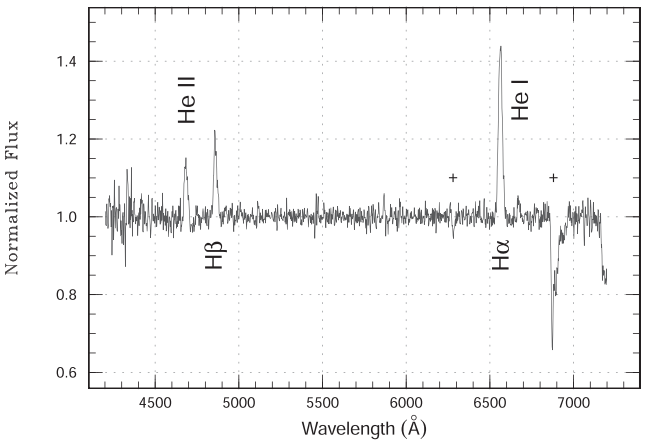

Fig. 7. Spectrum of BO Cet taken during the superoutburst on 2020 November 4. The "+" signs represent telluric absorptions.

Table 2. Equivalent width (EW) and full width at half maximum (FWHM) of our spectrum.

Hα		Hβ		He II 4686 Å	
EW	FWHM (Å)	EW	FWHM (Å)	EW	FWHM (Å)
12.4(1)	26.3(2)	4.7(1)	22.0(5)	3.2(1)	21.4(5)

where f ($0 < f < 1$) represents the distance between the center of the light center of the irradiated region from the center the mass of the secondary in unit of binary separation (Rodríguez-Gil et al. 2007b). Assuming the theoretical limit in which only the L_1 point is illuminated (a condition which is never actually achieved), f corresponds to the distance of the L_1 point from the center of the mass of the secondary (R_{L_2}). This extreme value is 0.383 for $q = 0.31$ and 0.392 for $q = 0.34$. The lower limit for f is achieved when the hemisphere is maximally irradiated and can be approximated by $f \simeq R_{L_2}^2$ (Rodríguez-Gil et al. 2007b). Using these values, we obtain $327 < K_2 < 542\,{\rm km\,s^{-1}}$. The mass of the white dwarf is constrained as $1.0 < M_1 < 4.7\,M_\odot$. Even taking the extreme limit of the maximum irradiation, the white dwarf is more massive than those in typical CVs; see e.g., $0.82(3)\,M_\odot$ in Zorotovic et al. (2011). This result is consistent with a suggestion of a massive white dwarf in the IW And-type postnova BC Cas (Kato & Kojiguchi 2020).

4.6 Spectroscopy

The result of snapshot spectroscopy is shown in figure 7. The equivalent widths (EW) and full widths at half maximum (FWHM) of strong lines are summarized in table 2.

In the spectrum of Zwitter and Munari (1995) during an apparent NL state, BO Cet showed a relatively strong He II emission. Compared to this, the current observation

seems to show a slightly enhanced He II emission, but the difference is subtle. A slight enhancement was probably due to the enhanced mass-accretion rate of the white dwarf during the superoutburst. The strong He II emission may be the result of a white dwarf in BO Cet being more massive than in ordinary CVs (subsection 4.5) [see Kimura et al. (2018) for examples of He II emission in DNe containing massive white dwarfs].

Rodríguez-Gil et al. (2007b) indicated that the Hα emission is singly peaked most of the time. The current observation also confirmed the singly peaked Hα emission despite the relatively high orbital inclination. We know that not all high-inclination dwarf novae show doubly peaked emission lines during superoutbursts, the best example being the WZ Sge-type dwarf nova V455 And (Nogami et al. 2009; Y. Tampo et al. in preparation). We consider that there may be a cause other than the SW Sex-type phenomenon producing singly peaked emission lines in light of the lack of signature of an SW Sex star in BO Cet in the orbital light curve (subsection 4.3).

5 Discussion

5.1 Mass ratio and SU UMa-type phenomenon

Although the q value (0.31–0.34) is expected to be normal for a binary with $P_{\rm orb} = 0.13983546$ d, this mass ratio is surprisingly large for an SU UMa star, since the 3 : 1 resonance is considered to be achieved only for $q < 0.25$ (Whitehurst 1988) or in extreme cases of 0.33 under temporary reduction of the mass transfer from the secondary (Murray et al. 2000). The recent results by Wakamatsu et al. (2021) also support that this limit is difficult to break, and that tidal truncation provides a hard limit for a disk to grow. However, since the secondary of BO Cet is not reported to be anomalous as in ASASSN-18aan (Wakamatsu et al. 2021; the lack of the secondary eclipse in BO Cet also excludes a luminous secondary as in ASASSN-18aan), the present results indicate that the limits presented by the past smoothed-particle hydrodynamics (SPH) simulations may not be as stringent as previously considered.

In fact, there has been yet another case of a super-long-period SU UMa star (MisV1448, $P_{\rm SH} = 0.237$ d, vsnet-alert 24912) most likely having $q > 0.30$.[8] Combined with ASASSN-14ho (Kato 2020), which had outburst characteristics very similar to MisV1448 (but without superhump detection), SU UMa stars above $q = 0.30$ had simply been missed by observations and may have simply been underestimated: observers tend to observe high-amplitude dwarf novae to establish the SU UMa-type nature while systems with high q have smaller outburst amplitudes; Z Cam stars have not usually been selected for time-resolved photometry in search of superhumps since it has been generally accepted that Z Cam-type and SU UMa-type categories are exclusive.

The treatment in the past SPH simulations also may have been responsible for this apparent discrepancy. According to Oyang, Jiang, and Blaes (2021), the viscosity in the disk, which is a reflection of the poloidal magnetic flux, determines the growth of eccentricity. It was possible that the past SPH simulations did not consider such an effect properly. Even in $q = 0.31$–0.34, the 3 : 1 resonance is within the tidal truncation radius (see subsection 5.2) and it is not logically impossible to excite the 3 : 1 resonance under these high q values.

5.2 Origin of superoutbursts

We compared the radius of the 3 : 1 resonance [$r_{3:1} = 3^{-2/3}(1+q)^{-1/3}A$] and tidal truncation radius. We used the approximated formula of tidal truncation radius $r_{\rm tidal} = 0.60/(1+q)A$ for $0.03 < q < 1$ given by Paczyński (1977).

For $q = 0.31$, these values are $r_{3:1} = 0.440A$ and $r_{\rm tidal} = 0.46A$. For $q = 0.34$, they are $0.436A$ and $0.45A$, respectively. It is worth noting that $r_{3:1}$ and $r_{\rm tidal}$ are critically close in the parameter of BO Cet. The disk radius during standstills in IW And stars is known to increase at in least two studies (Kimura et al. 2020a; M. Shibata et al. in preparation). The same is true for the only previously known Z Cam/SU UMa star NY Ser (Kato et al. 2019). Furthermore, direct observational determination of the disk radius by M. Shibata et al. (in preparation) indicates that IW And-type standstills are terminated by brightening when the disk radius eventually reaches the tidal truncation radius, in the same way as the radius 3 : 1 resonance performs in SU UMa stars. It looks likely that there exists a mechanism of effective removal of angular momentum at the tidal truncation radius [see also a discussion in subsection 4.1 in Kimura et al. (2020a)].

In BO Cet, this removal of angular momentum probably starts to work when the disk expands to the tidal truncation radius during a standstill, and a standstill ends up with IW And-type brightening often followed by a deep dip.

In figure 1, IW And-type brightening at the end of standstills reached a constant magnitude of 14.0.[9] This fixed brightness can be regarded as a signature of the disk reaching the tidal truncation radius and the associated effective removal of the angular momentum working. In the DN phase in 2020 before BJD 2459140, however, this limit of 14.0 mag was surpassed several times (figure 2), suggesting

[8] ⟨http://ooruri.kusastro.kyoto-u.ac.jp/mailarchive/vsnet-alert/24912⟩.

[9] The ASAS-SN and our CCD magnitudes can be regarded as the same for the disk-dominated ($B - V \sim 0$) system BO Cet.

that the disk expanded beyond the tidal truncation radius. This is likely due to thermal instability causing the disk to expand due to increased viscosity under the condition of the angular momentum conservation. In the IW And phase, such a large variation of viscosity is not expected during standstills and the absence of superoutbursts starting from standstills appears to be explained by the inability of the disk expanding beyond the tidal truncation radius. Even if the disk radii apparently exceeded the tidal truncation radius (and probably reaches the radius of the 3 : 1 resonance) during some outbursts in the DN phase, only one or two outbursts eventually became superoutbursts. This was probably because tidal instability at the 3 : 1 resonance requires time to develop (cf. Lubow 1991a, 1991b) and only long-lasting outbursts could eventually develop tidal instability to manifest the SU UMa-type feature.

5.3 Unsolved questions

Although the phenomenon observed in BO Cet appears to be explained by a chance (nearly) superposition of $r_{3:1}$ and $r_{\rm tidal}$, there remain a number of unknowns. We summarize them as hints to future studies in the understanding of the accretion disks in dwarf novae.

- Relation between IW And and SU UMa phenomena. Both IW And and SU UMa phenomena are powered by the presence of a characteristic disk radius at which either IW And-type brightening or an SU UMa-type superoutburst occurs. Do the underlying mechanisms in these systems have something in common?
- Interaction of the phenomena at $r_{3:1}$ and $r_{\rm tidal}$. In SU UMa stars with large q, the development of superhumps is known to be slow (Kato et al. 2014, 2016). Could this be a result of competition or interference between tidal instability at the radius of the 3 : 1 resonance and tidal truncation? Alternatively, could the 3 : 1 resonance affect the behavior when the disk radius reaches the tidal truncation radius in systems that have similar q to BO Cet?
- Why do few systems with intermediate q show superoutbursts? Not all systems with intermediate q (0.25–0.35) have shown superoutbursts. What is the difference between BO Cet and other systems? Is the case of BO Cet related to the condition allowing IW And-type phenomenon to occur, which, however, is still poorly understood?

6 Summary

We observed BO Cet, which had been considered as a novalike CV. During the 2020–2021 season, the object showed dwarf nova-type outbursts and superhumps that had a period 7.8% longer than the orbital one developed at least during one long outburst. This object has thus been confirmed as an SU UMa-type dwarf nova with an exceptionally long orbital period [0.13983546(3)].

Furthermore, we found that the object showed IW And-type variation in 2019–2020 in the archival data, which is characterized by (often repetitive) slowly rising standstills terminated by brightening. This object is thus the first CV showing both SU UMa-type and IW And-type features.

We found that the object is eclipsing and estimated the orbital inclination to be 72(1)°. Using the published radial-velocity study, we constrained the mass of the white dwarf larger than 1.0 $M_\odot$. This supports the previous claim that the IW And-type phenomenon (in some objects) may be associated with the high mass of the white dwarf. The massive white dwarf may also be responsible for the strong He II line in the spectra.

We obtained a mass ratio of 0.31–0.34 from the superhumps in the growing phase (stage A superhumps). At this mass ratio, the radius of the 3 : 1 resonance, responsible for tidal instability and superhumps, and the tidal truncation radius are very similar and might lead to the unusual behavior in this object.

We interpret that in some occasions this object showed IW And-type variation when the disk size was not large enough but that the radius of the 3 : 1 resonance could be reached as a result of thermal instability. The reason, however, why this object is unique in that it shows both SU UMa-type and IW And-type features is still unsolved.

Supplementary data

The following supplementary data is available at PASJ online.

E-figures 1–2 and e-table 1.

Acknowledgments

The author is particularly grateful to the ASAS-3 and ASAS-SN team for making their data available to the public. We acknowledge with thanks the variable star observations from the AAVSO International Database contributed by observers worldwide and used in this research. This research has made use of the International Variable Star Index (VSX) database, operated at AAVSO, Cambridge, Massachusetts, USA. We also benefited from the data by Filipp Romanov. This work was supported by JSPS KAKENHI Grant Number 21K03616.

References

Bruch, A. 2017, New Astron., 52, 112
Cleveland, W. S. 1979, J. Am. Statist. Assoc., 74, 829

Fernie, J. D. 1989, PASP, 101, 225
Gaia Collaboration, 2018, A&A, 616, A1
Hameury, J.-M., & Lasota, J.-P. 2014, A&A, 569, A48
Kato, T. 2019, PASJ, 71, 20
Kato, T. 2020, PASJ, 72, L2
Kato, T., et al. 2009, PASJ, 61, S395
Kato, T., et al. 2010, PASJ, 62, 1525
Kato, T., et al. 2013, PASJ, 65, 23
Kato, T., et al. 2014, PASJ, 66, 90
Kato, T., et al. 2016, PASJ, 68, L4
Kato, T., et al. 2019, PASJ, 71, L1
Kato, T., Hambsch, F.-J., Oksanen, A., Starr, P., & Henden, A. 2015, PASJ, 67, 3
Kato, T., & Kojiguchi, N. 2020, PASJ, 72, 98
Kato, T., & Osaki, Y. 2013, PASJ, 65, 115
Kato, T., Uemura, M., Ishioka, R., Nogami, D., Kunjaya, C., Baba, H., & Yamaoka, H. 2004, PASJ, 56, S1
Kimura, M., et al. 2018, PASJ, 70, 78
Kimura, M., Osaki, Y., & Kato, T. 2020a, PASJ, 72, 94
Kimura, M., Osaki, Y., Kato, T., & Mineshige, S. 2020b, PASJ, 72, 22
Kochanek, C. S., et al. 2017, PASP, 129, 104502
Kurita, M., et al. 2020, PASJ, 72, 48
Lima, I. J., et al. 2021, AJ, 161, 225
Lubow, S. H. 1991a, ApJ, 381, 259
Lubow, S. H. 1991b, ApJ, 381, 268
Matsubayashi, K., et al. 2019, PASJ, 71, 102
Meyer, F., & Meyer-Hofmeister, E. 1983, A&A, 121, 29
Murray, J., Warner, B., & Wickramasinghe, D. 2000, New Astron. Rev., 44, 51
Nogami, D., et al. 2009, in ASP Conf. Ser., 404, The Eighth Pacific Rim Conference on Stellar Astrophysics: A Tribute to Kam-Ching Leung, ed. S. J. Murphy & M. S. Bessell (San Francisco: ASP), 52
Osaki, Y. 1996, PASP, 108, 39
Osaki, Y., & Kato, T. 2013, PASJ, 65, 95
Oyang, B., Jiang, Y.-F., & Blaes, O. 2021, MNRAS, 505, 1
Paczyński, B. 1977, ApJ, 216, 822
Pojmański, G. 2002, Acta Astron., 52, 397
Rodríguez-Gil, P., et al. 2007a, MNRAS, 377, 1747
Rodríguez-Gil, P., Schmidtobreick, L., & Gänsicke, B. T. 2007b, MNRAS, 374, 1359
Samus, N. N., et al. 2011, VizieR Online Data Catalog, B/gcvs
Shappee, B. J., et al. 2014, ApJ, 788, 48
Simonsen, M. 2011, J. Am. Assoc. Variable Star Obs., 39, 66
Stellingwerf, R. F. 1978, ApJ, 224, 953
Thorstensen, J. R., Davis, M. K., & Ringwald, F. A. 1991, AJ, 102, 683
Wakamatsu, Y., et al. 2021, PASJ, 73, 1209
Warner, B. 1995, Cataclysmic Variable Stars (Cambridge: Cambridge University Press)
Whitehurst, R. 1988, MNRAS, 232, 35
Zorotovic, M., Schreiber, M. R., & Gänsicke, B. T. 2011, A&A, 536, A42
Zwitter, T., & Munari, U. 1995, A&AS, 114, 575